J. Basic Sci. Appl. Res., 1(3)1-10, 2015

ISSN 2356-8879
Journal of Basic Sciences and Applied Research
www.textroad.com

Modeling of GPR Profile: An Example from Archaeological Site in Basrah, Iraq

Hazim A Alaamer

University of Basrah, Earth Science Dept.

ABSTRACT

GPR profiles conceptualize remains of archaeological site in Basrah have been created using finite difference time domain modeling. Dimension and architecture of the remains were taken from satellite aerial image of Google Earth application. The Modeling follows a gradual approach to simulate the remains as it were buried with focus to show the effect of surface roughness introduced to the constituent objects of the model. Results of the modeling vary from simple reflection from the buried structure to complex interaction of electromagnetic wave with subsurface conditions. Implication of roughness introduced can be seen in magnifying the attenuation, and subsequently reducing the depth of penetration.

KEY WORDS: GPR, FDTD, Archaeological, Modeling

INTRODUCTION

Solving subsurface problems in the field of archaeology without destructively intervening with the buried materials has become a prime focus of the archaeological community [6]. An important distinguishing feature of Ground penetrating Radar- GPR- is that the method is easy to use and is neither destructive nor invasive; this makes it suitable for use also in urban settings and archaeological environments [11]. The first application of GPR in archaeology was initiated soon after the first commercial equipment became available in 1970 [6]. Historically, some claim that Basrah is the home of the mythical Sinbad the Sailor, and others claim that it is the actual location of the Garden of Eden. It is known for certain that the Umar Ibn Al-Khattab, a companion of the Prophet Muhammad and one of the most influential of the four Rashidun Caliphs, defeated Persian armies from the Sassanid Empire. Shortly after this victory, Basrah city's first foundations were laid in 636 CE (14 AH), just a few kilometers south of the present-day location. Basrah was officially founded along with Kufa, Najaf, as a twin garrison town only two years later [8] (figure 1). The first attempt to study the archaeological site in Basrah was carried out by Sabti & Mutasher (2006) [9]. Of all current research areas in GPR, numerical modeling is arguably one of the most popular, with increasing number of publications containing some forms of numerical modeling in their content [6]. The finite difference time domain-FDTD- technique has become one of the most common in the past few years, particularly with the rapid increase in accessible and inexpensive computational resources [3]. The aim of the study is, first, to simulate the electromagnetic wave field response over a known archaeological site in Basrah, with aid of FDTD modeling, as it were buried and later investigated by GPR antenna of 250 MHz. The second is to establish a realistic approach via modeling of expected conditions of the site, in particular the effect of roughness on GPR image.

* **Corresponding Author:** Hazim A Alaamer, University of Basrah, Earth Science Dept.
Alaamer74@yahoo.com

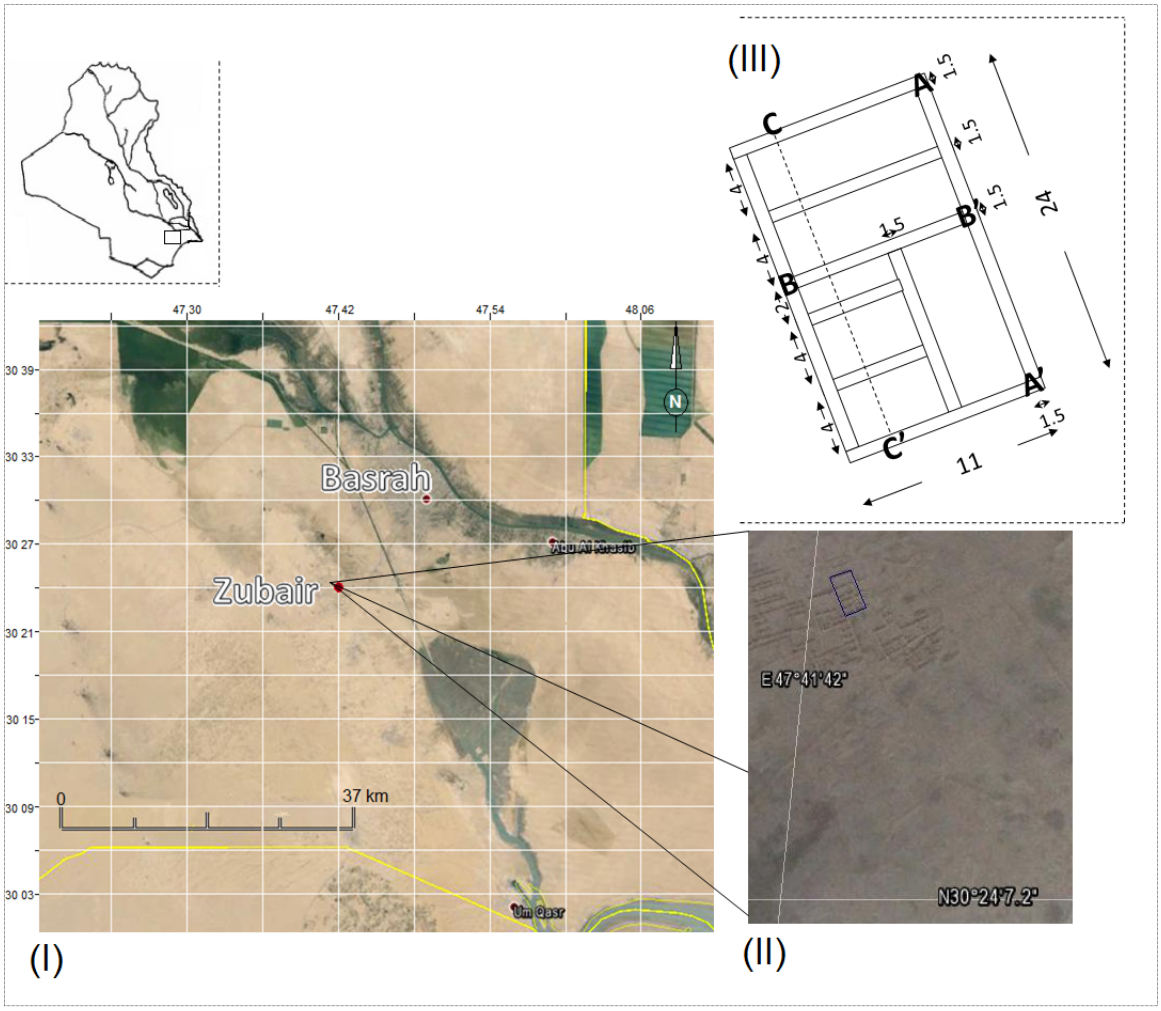

Figure1: (I) Location map, (II) Map of the archaeological site, blue rectangle is part of the site selected for modeling, dimensions and proposed view seen from Google Earth are shown in (III).

Theory:

1- Electromagnetic wave:

Considering a region of space that has no electric or magnetic current sources, but it may have materials that absorb electric or magnetic energy field. The time dependent of Maxwell's equations are given [12]:

Faraday's Law

$$\frac{\partial \mathrm{B}}{\partial t} = -\nabla \times \vec{E} - \vec{M} \qquad \ldots\ldots\ldots\ldots\ldots 1\text{-}1$$

Ampere's Law

$$\frac{\partial D}{\partial t} = \nabla \times \vec{H} - \vec{J} \qquad \ldots\ldots\ldots\ldots\ldots\ldots 1\text{-}2$$

Gauss's Law for Electric field

$$\nabla . \vec{D} = 0 \qquad \ldots\ldots\ldots\ldots\ldots\ldots 1\text{-}3$$

Where $\vec{E}$ =electric field (volts/meter), $\vec{D}$= electric flux density (coulombs/meter^2), $\vec{H}$=magnetic field (amperes/meter), $\vec{B}$=magnetic flux density (Weber/meter^2), $\vec{J}$=electric current density (ampere/meter^2), $\vec{M}$ =equivalent magnetic current density (volt/meter^2). In linear, isotropic, non-dispersive materials, we can relate $\vec{D}$ to $\vec{E}$ and $\vec{B}$ to $\vec{H}$ using simple proportions:

$$\vec{D} = \varepsilon \vec{E} = \varepsilon_{\circ}\varepsilon_r \vec{E} \qquad \ldots\ldots\ldots\ldots\ldots\ldots\ldots\ldots 1\text{-}4$$

$$\vec{B} = \mu \vec{H} = \mu_r \mu_{\circ} \vec{H} \qquad \ldots\ldots\ldots\ldots\ldots\ldots\ldots\ldots 1\text{-}5$$

Where ε=electrical permittivity (farad/meter), ε_r=relative permittivity (dimensionless), ε_o=free space permittivity (8.854 x 10^{-12} farad/meter), μ=magnetic permeability (Henry/meter), μ_r=relative magnetic permeability (dimensionless), μ_o= free space permeability (4π x 10^{-7} Henry/meter). $\vec{J}$ & $\vec{M}$ can act as independent sources of E and H energy, $\vec{J}_{source}$ &$\vec{M}_{source}$, this yields:

$$\vec{J} = \vec{J}_{source} + \sigma\vec{E} \quad \text{.....1-6}$$

$$\vec{M} = \vec{M}_{source} + \sigma^*\vec{H} \quad \text{.....1-7}$$

Where σ=electric conductivity (siemen/meter), σ^*=equivalent magnetic loss (ohms/meter). The Maxwell's curl equations can be obtained by substituting equations 1-6 and 1-7into equations 1-1 and 1-2 [12]:

$$\frac{\partial\vec{H}}{\partial t} = -\frac{1}{\mu}\nabla\times\vec{E} - \frac{1}{\mu}\left(\vec{M}_{source} + \sigma^*\vec{H}\right) \quad \text{.....1-8}$$

$$\frac{\partial\vec{E}}{\partial t} = \frac{1}{\varepsilon}\nabla\times\vec{H} - \frac{1}{\varepsilon}\left(\vec{J}_{source} + \sigma\vec{E}\right) \quad \text{.....1-9}$$

In Cartesian coordinates, this yields the following system of six coupled scalar equations [12]:

$$\frac{\partial H_x}{\partial t} = \frac{1}{\mu}\left[\frac{\partial E_y}{\partial z} - \frac{\partial E_z}{\partial y} - \left(M_{source_x} + \sigma^* H_x\right)\right] \quad \text{.....1-10}$$

$$\frac{\partial H_y}{\partial t} = \frac{1}{\mu}\left[\frac{\partial E_z}{\partial x} - \frac{\partial E_x}{\partial z} - \left(M_{source_y} + \sigma^* H_y\right)\right] \quad \text{.....1-11}$$

$$\frac{\partial H_z}{\partial t} = \frac{1}{\mu}\left[\frac{\partial E_z}{\partial y} - \frac{\partial E_y}{\partial x} - \left(M_{source_z} + \sigma^* H_z\right)\right] \quad \text{.....1-12}$$

$$\frac{\partial E_x}{\partial t} = \frac{1}{\varepsilon}\left[\frac{\partial H_z}{\partial y} - \frac{\partial H_y}{\partial z} - \left(J_{source_x} + \sigma E_x\right)\right] \quad \text{.....1-13}$$

$$\frac{\partial E_y}{\partial t} = \frac{1}{\varepsilon}\left[\frac{\partial H_x}{\partial z} - \frac{\partial H_z}{\partial x} - \left(J_{source_y} + \sigma E_y\right)\right] \quad \text{.....1-14}$$

$$\frac{\partial E_z}{\partial t} = \frac{1}{\varepsilon}\left[\frac{\partial H_y}{\partial x} - \frac{\partial H_x}{\partial y} - \left(J_{source_z} + \sigma E_z\right)\right] \quad \text{.....1-15}$$

If the incident wave is also uniform in the z-direction, then all partial derivatives of the fields with respect to z must be zero [4]. In this regard, the plane electromagnetic field can be decomposed into transverse electric-TE, and transverse magnetic-TM [4]. Then, the full set of Maxwell's curl equations reduces to [12]:

$$\frac{\partial H_x}{\partial t} = \frac{1}{\mu}\left[-\frac{\partial E_z}{\partial y} - \left(M_{source_x} + \sigma^* H_x\right)\right] \quad \text{.....1-16}$$

$$\frac{\partial H_y}{\partial t} = \frac{1}{\mu}\left[-\frac{\partial E_z}{\partial x} - \left(M_{source_y} + \sigma^* H_y\right)\right] \quad \text{.....1-17}$$

$$\frac{\partial H_z}{\partial t} = \frac{1}{\mu}\left[\frac{\partial E_x}{\partial y} - \frac{\partial E_y}{\partial x} - \left(M_{source_z} + \sigma^* H_z\right)\right] \quad \text{.....1-18}$$

$$\frac{\partial E_x}{\partial t} = \frac{1}{\varepsilon}\left[\frac{\partial H_y}{\partial z} - \left(J_{source_x} + \sigma E_x\right)\right] \quad \text{.....1-19}$$

$$\frac{\partial E_y}{\partial t} = \frac{1}{\varepsilon}\left[-\frac{\partial H_z}{\partial x} - \left(J_{source_y} + \sigma E_y\right)\right] \quad \text{.....1-20}$$

$$\frac{\partial E_z}{\partial t} = \frac{1}{\varepsilon}\left[\frac{\partial H_y}{\partial x} - \left(J_{source_z} + \sigma E_z\right)\right] \quad \text{.....1-21}$$

2- Finite Difference Time domain Modeling:

In practice, the volume to be modelled is sub-divided into a three-dimensional grid (usually orthogonal) of individual 'field cells' of dimensions Δx, Δy, Δz. Within each cell, the electrical field (E) and the magnetic field (H) are described by component Cartesian E(x, y, z) and H(x, y, z) field vectors staggered in space in a manner that is referred to as 'Yee cell' geometry. With the use of a finite-difference approximation to the differential form of Maxwell's electromagnetic field equations, it is possible to calculate the electric field at any point in space, and time, from a knowledge of its neighboring magnetic fields, and vice versa [3]. With reference to Yee cell, see [12], [3] and [10], and considering TM wave, then the corresponding finite difference relations are [4]:

$$E_{z(i,j)}^{n+1} = \left[\frac{1-\sigma\Delta t/2\varepsilon}{1+\sigma\Delta t/2\varepsilon}\right]E_{z(i,j)}^{n} + \frac{\Delta t/\varepsilon\Delta}{1+\sigma\Delta t/2\varepsilon}\left[H_{y(i+1,j)}^{n+1} - H_{y(i-1,j)}^{n+1} + H_{x(i,j-1)}^{n+1} - H_{x(i,j+1)}^{n+1}\right] \quad \text{.....1-22}$$

$$H_{x(i,j+1)}^{n+1} = \left[\frac{1-\sigma^*\Delta t/2\mu}{1+\sigma^*\Delta t/2\mu}\right]H_{x(i,j+1)}^{n-1} + \frac{\Delta t/\mu\Delta}{1+\sigma^*\Delta t/2\mu}\left[E_{z(i,j)}^{n} - E_{z(i,j+1)}^{n}\right] \quad \text{.....1-23}$$

$$H_{y(i+1,j)}^{n+1} = \left[\frac{1-\sigma^*\Delta t/2\mu}{1+\sigma^*\Delta t/2\mu}\right]H_{y(i+1,j)}^{n-1} + \frac{\Delta t/\mu\Delta}{1+\sigma^*\Delta t/2\mu}\left[E_{z(i,+1j)}^{n} - E_{z(i,j)}^{n}\right] \quad \text{.....1-24}$$

Where Δt is time increment, and Δ is a small increment and it is usually denoted a space grid points [4]:

$(i,j,k)= (i\Delta x, j\Delta y, k\Delta z)$, note that the $k\Delta z$ is not included in equations 1-22, 1-23 and 1-24 because we assume that $\partial/\partial z=0$.

METHODOLOGY

We started our work by selecting a representative site to model a GPR profile(figure 1, II) at this stage, the key issue in site selection is the site has pronounced features, for example walls, that can be seen protruding from the ground enough. This will facilitate later measurement of the site geometry and dimensions. Utilizing from Google Earth, we choose the site shown in figure 1 II & III, and as a result, site dimensions can be determined. From figure 1-III-, the length is 24 meters, from point A to A', and the width is 11 meters, from point B to B'. Wall thickness is taken to be approximately 1.5 meter. The purpose is to model a profile along the line from C-C. (Figure 1-III-). For the model to be rational, three assumptions have been made of which must meet the following facts:

1- Basrah Region is characterized by humid, hot weather with relatively high water table level [8]& [2].
2- From observations, building materials of the archaeological site are mud or partially cured mud bricks.

The assumptions about the model are:

1- The site was leveled to the ground and only small portion near the base of the walls remained.
2- The wall materials, as well as the floors, are moist so that the conductivity and dielectric constant are reasonably high.
3- The site was buried by sediments, mainly sand, that could produce dielectric constant enough to be differentiated from the wall materials.

These assumptions are discussed later in the text. The modeling was sub-divided into three steps. For each step, modeling parameters are kept constant and listed in table 1. As we progress in the steps, we introduce a new factor in the model till we have developed the final model, step 3. The principle factor that we believe to perturb the subsurface GPR image is the roughness of the surfaces from which the electromagnetic signal are reflected. The main scheme to produce the synthetic GPR profile relies on finite difference time domain modeling, FDTD, operating with MATLAB. Because the simulation process is time consuming, especially with fine time and space increments, efficient computer is highly demanded when running these models.

Table 1: parameters and values of time and space increments implemented in the modeling

Parameter	Value
Trace spacing (dx)	0.069 meter
Depth spacing(dz)	0.017 meter
Source start point	0 meter
Source spacing	0.69 meter
Sampling interval(dt)	0.45 nano-second
Total two travel time	26.67 nano-second

The line C-C' of the draft archaeological structure shown in figure 1-III- is the main theme for modeling. The synthetic profile's length is 30 meters with depth extends up to 3 meters. All the models contain an air gap of 0.05 meter to simulate the practical application of GPR mounted on cart, for instance Mala GPR 250 MHz. Wall width was 1.5 meter, and wall separation ranges from 2 to 4 meters depending on the architecture style observed from figure 1-III-.

1- Model 1 (Modeling of 250 MHz frequency without roughness factor):

Figure (2) depicts the proposed model without roughness factor. In this step, wall dimensions are uniform with 0.3 meter depth extent and 1.5 meter width. Floors thickness is also fixed and uniform at 0.05 meter thick. Depth of burial measured from air-sand interface, ground surface; to the top surface for each is 0.1 meter. Floors depth of burial measured from the same interface is 0.15 meter. This gives a relief of 0.05 meter between wall and floor top surfaces. The resultant synthetic GPR profile is shown in figure (3). Diffractions from the walls can be identified clearly as well as the multiples from the floors.

2- Model 2 (Modeling with 250 MHz frequency with roughness factor added to the floors):

Figure (4) illustrates the model with roughness factor added to the floors that intervene the walls. The roughness was random and uncorrelated from floor to another. Wall width and thickness is similar to that of step 1. The result of the simulation is shown in figure (5). Here, it is evident that the diffractions caused

by floor surface roughness overlap with the ones of the walls in a manner that poses difficult identification between them.

3- Model 3 (Modeling with 250 MHz frequency with roughness added to walls and floors):

Figure (6) shows the same archeological model in figure (2), but the roughness in this step has been added to walls and floors as well. The result of the simulation using finite difference time domain modeling is shown in figure (7). In step 2, the diffraction overlap caused by roughness rendered the synthetic profile hard to interpret. Now, it becomes even harder to distinguish reflections from the walls and floors.

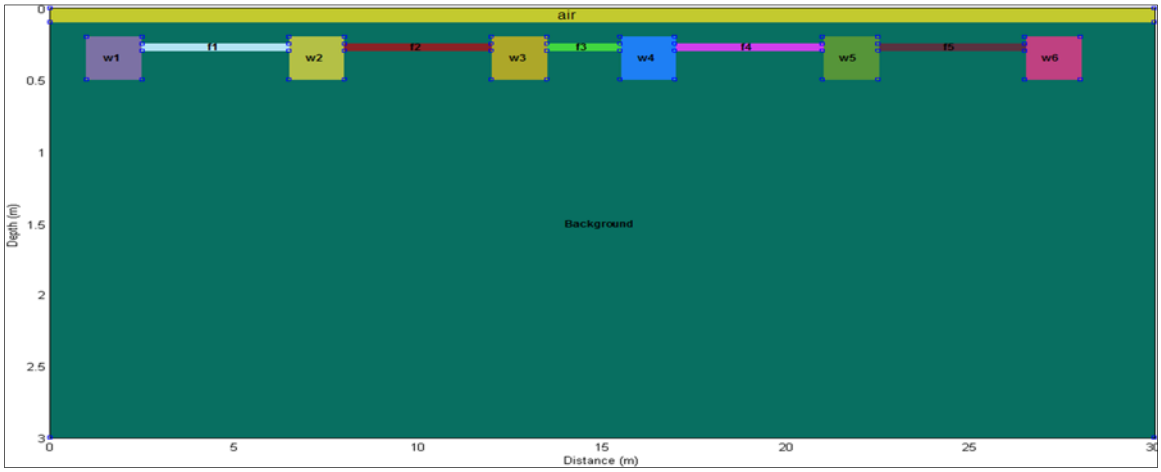

Figure 2: Earth model 1, letters designate buried objects, 'w' for wall and 'f' for floor.

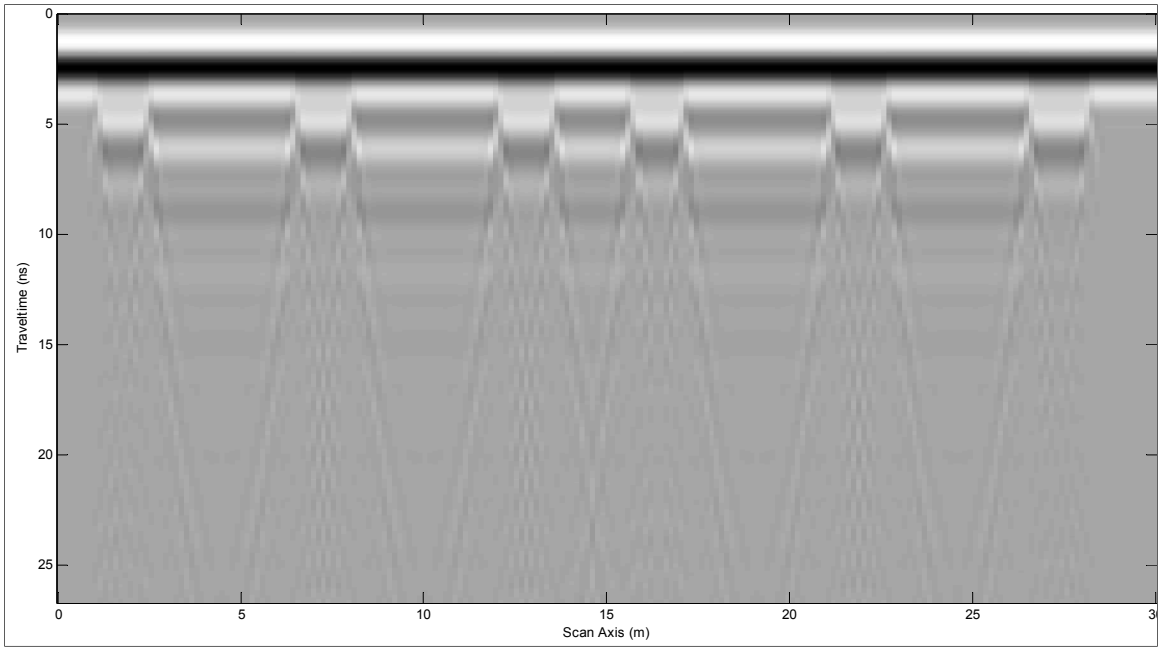

Figure 3: Synthetic GPR profile resulted from model1, frequency 250 MHz with no roughness added to the subsurface.

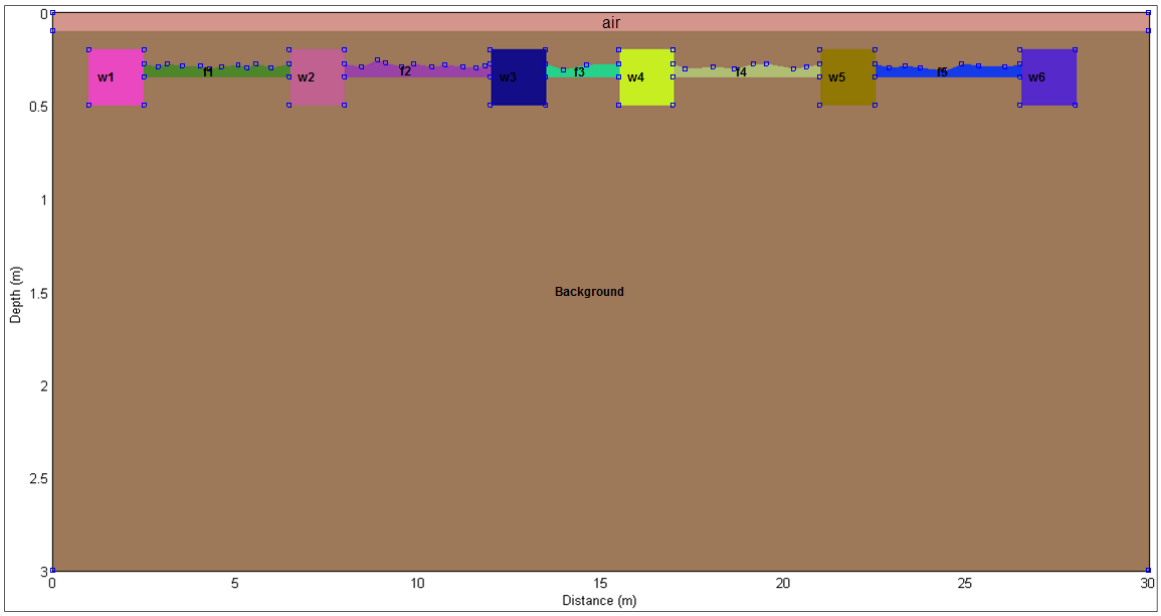

Figure 4: Earth model 2, letters designate buried objects, 'w' for wall and 'f' for floor. Notice the rugged surface of the floors representing roughness factor.

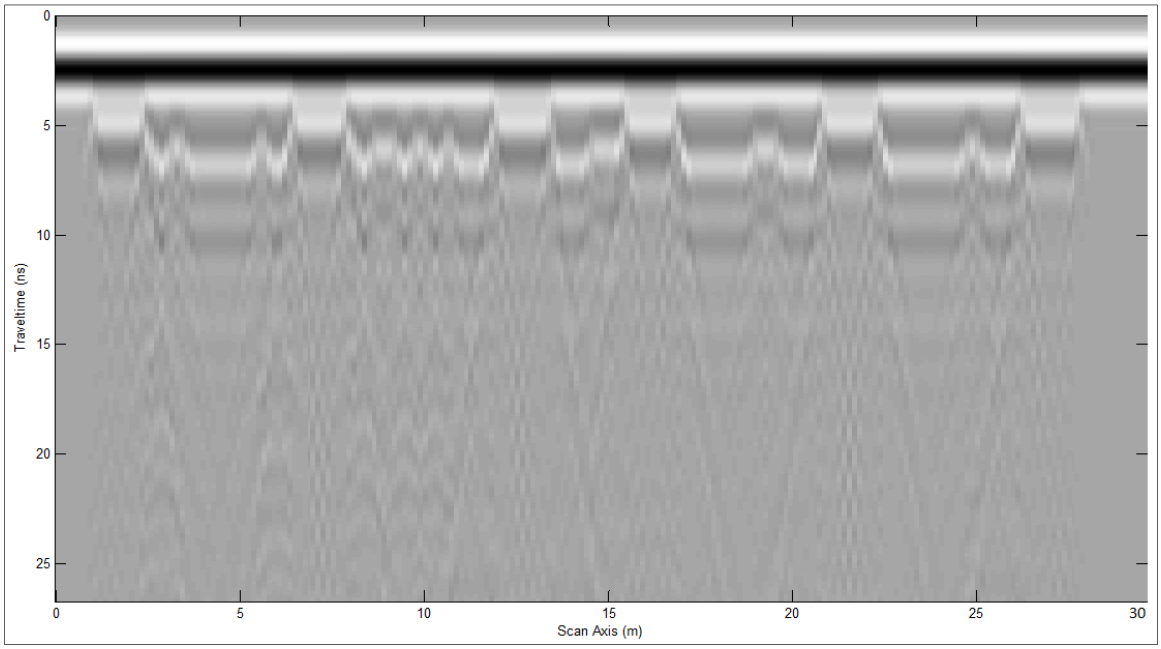

Figure 5: Synthetic GPR profile resulted from model 2, 250 MHz. Diffractions from walls and floors overlap because of rugged floor surfaces. Reflections from relatively high protrusions of rugged floor surfaces might be confused with wall, especially to the right of the profile between 19-25 meters distance.

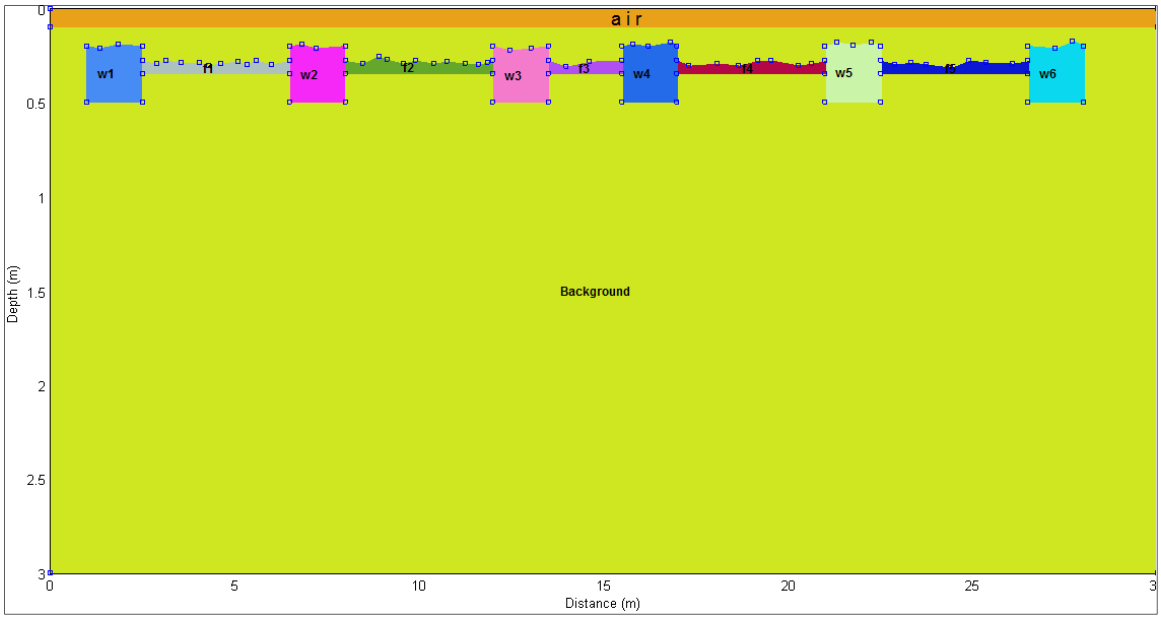

Figure 6: Earth model 3, letters designate buried objects, 'w' for wall and 'f' for floor. Rugged surfaces added for both walls and floors to simulate roughness factor.

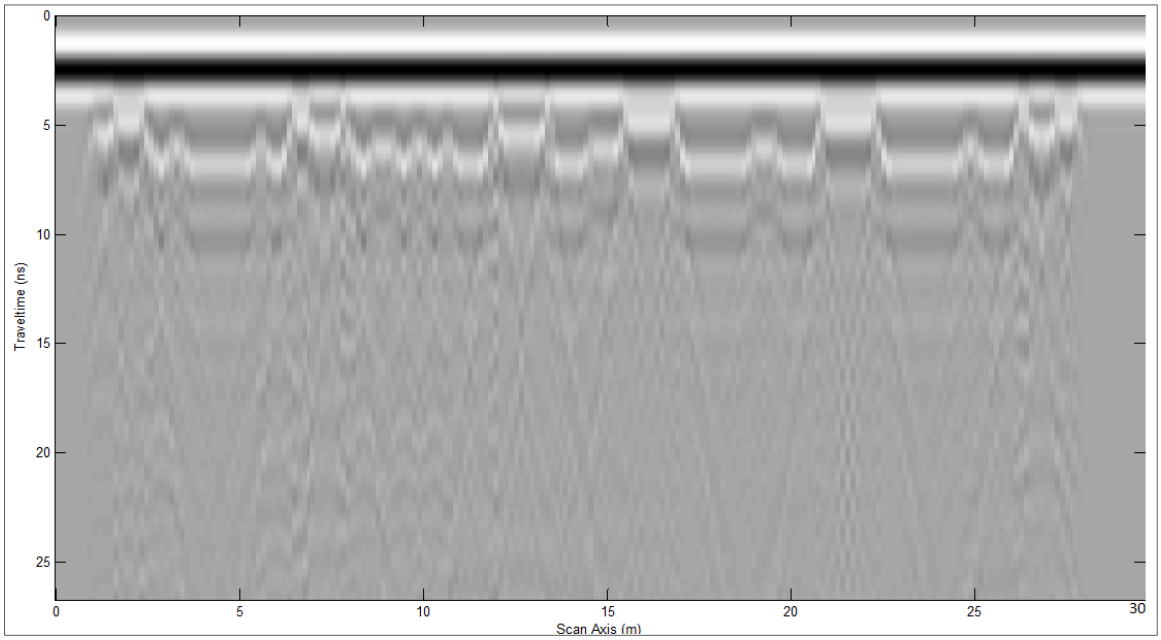

Figure 7: Synthetic GPR profile resulted from model 3, 250 MHz. Rugged surfaces added to walls and floors make discrimination between walls and floors difficult, especially at locations to the left of the profile between 2-9 meters distance and to the most right between 25-28 meters distance.

DISCUSSION

The length of all synthetic GPR profiles present in this work is 30 meters. However, the length of line C-C' in figure 1-III- is 24 meters. It is necessary to see areas that have no anomalies and to bring visual value to the surveyed areas that do.[3]. For comparison, figure (8) represents real GPR data acquired over archaeological location where the survey grid was so restricted to allow full visualization to the anomaly at

the top left of the profile. Concerning velocity and depth determination, one method involved in this regard is matching of shapes of hyperbolas detected on the GPR [6]. With respect to figure (7), at first glance, it is a daunting job trying to match hyperbola shape for single object. Surface roughness introduced to the model complicated the process of hyperbola fitting completely. The process; i.e. hyperbola matching, requires a flat reflector at depth and relatively homogenous materials over the length of the field measurement [6]. For such environment, for example archaeology investigation, one should resort to other methods of velocity and depth determination such as laboratory measurement of dielectric and conductivity, and wide angle measurement using separated transmitter and receiver antenna [6]. For models shown here, the assigned values of the conductivity and dielectric constant along with calculated velocities are listed in table 2.

Table 2: values of dielectric, resistivity and velocity assigned to the models

parameter	wall	floor	background	air
Velocity (m/ns)	0.001581	0.001581	0.12239	0.3
Dielectric constant	3	3	6	1
Magnetic permeability(H/m)	1	1	1	1
Resistivity (Ω/m)	0.001	0.001	1000	∞

.

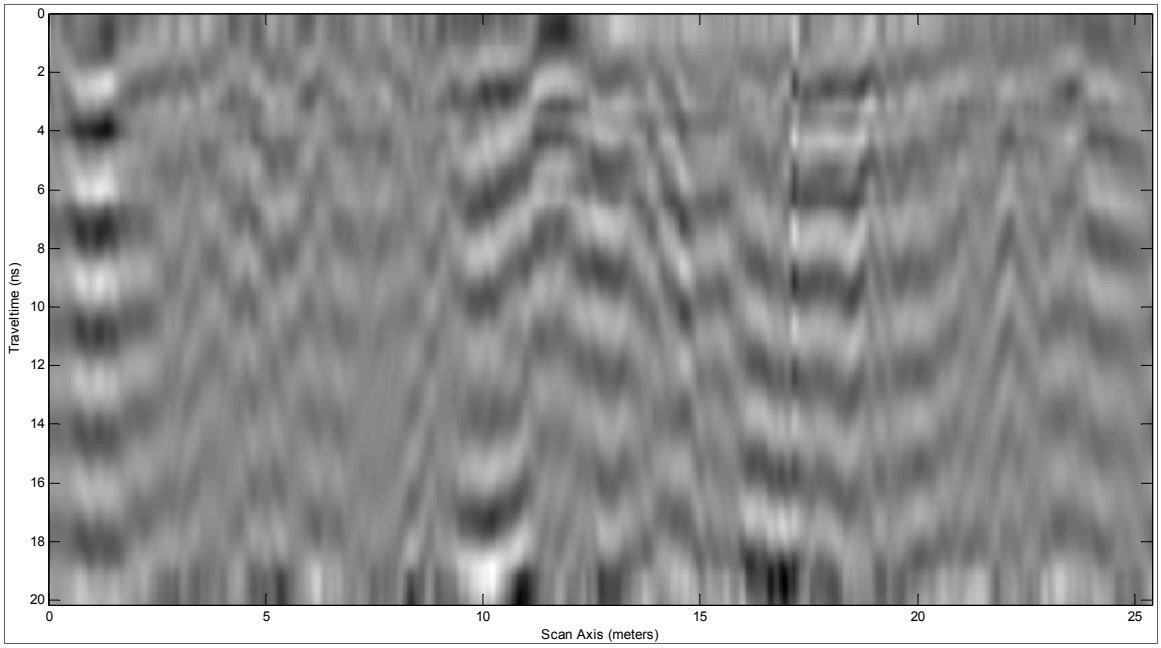

Figure 8: Real GPR data from archaeological location. Antenna frequency is 250 MHz.

In table 2, the equation used in velocity calculation is:

$$v = \frac{C}{\sqrt{\varepsilon_r}}$$

C is velocity of light (0.3 m/ns) and ε_r is the relative dielectric permittivity. The conductivity ($\sigma=1/\rho$) of a material is defined as the reciprocal of the resistivity ρ [11]. Skin depth, sometimes referred to as depth of penetration of electromagnetic wave can be obtained from [11]:

$$\delta = \frac{2}{\sigma}\sqrt{\frac{\varepsilon}{\mu}}$$

'μ' is the magnetic permittivity. It follows from the equation above that the electrical conductivity is the most important variable controlling the depth of penetration [11]. Conductivity of varying soil materials also has a wide dispersion since the conductivity drastically changes by any inclusion of water or moisture into the soil [3]. With reference to [7], [2], [1] and [13], we are driven to infer that the conductivity of the

main constituents of the models; i.e. walls and floors, is relatively high. And, there is no indication of the opposite. Consequently, the resistivity values assigned to these constituents are adversely low (table 2).

Figure (9) illustrates the mean and the median attenuation as a function of time. The effect of roughness is comparable from model to another. Increasing surface roughness results in more attenuation by considerable proportion in which the effect can be noticed remarkably after 8-10 nano-seconds, the time corresponds to buried structure in the models (figures 2, 4, 6). Here, surface roughness contributes to additional attenuation of which has direct relation to penetration depth; reference can be made to the following equation [11]:

$$\frac{1}{\alpha} = \delta = \left(\frac{2}{\sigma}\right)\left(\frac{\varepsilon}{\mu_\circ}\right)^{\frac{1}{2}}$$

Here,α is the attenuation and δ is the skin depth. It is worthy to mention that all models did not account for roughness at air-ground interface. Choice of simplification with other matters related to limited computational resource has been a subject of consideration in this regard. Otherwise, effects of ground surface depression and protrusions have influence in reduction the wavelength that makes the rough surface appears electrically larger [3]. To turn to interpretation, the interesting thing that a mere look to figure (7) without consulting the model from which the GPR profile was created, can be exhausted job, in particular, the case where many profiles exhibit the same pattern. Hence, highlighting the importance of modeling, mathematical modeling has become increasingly popular interpretation tool; and is often used in conjunction with many of the more traditional signal or image processing technique [3].

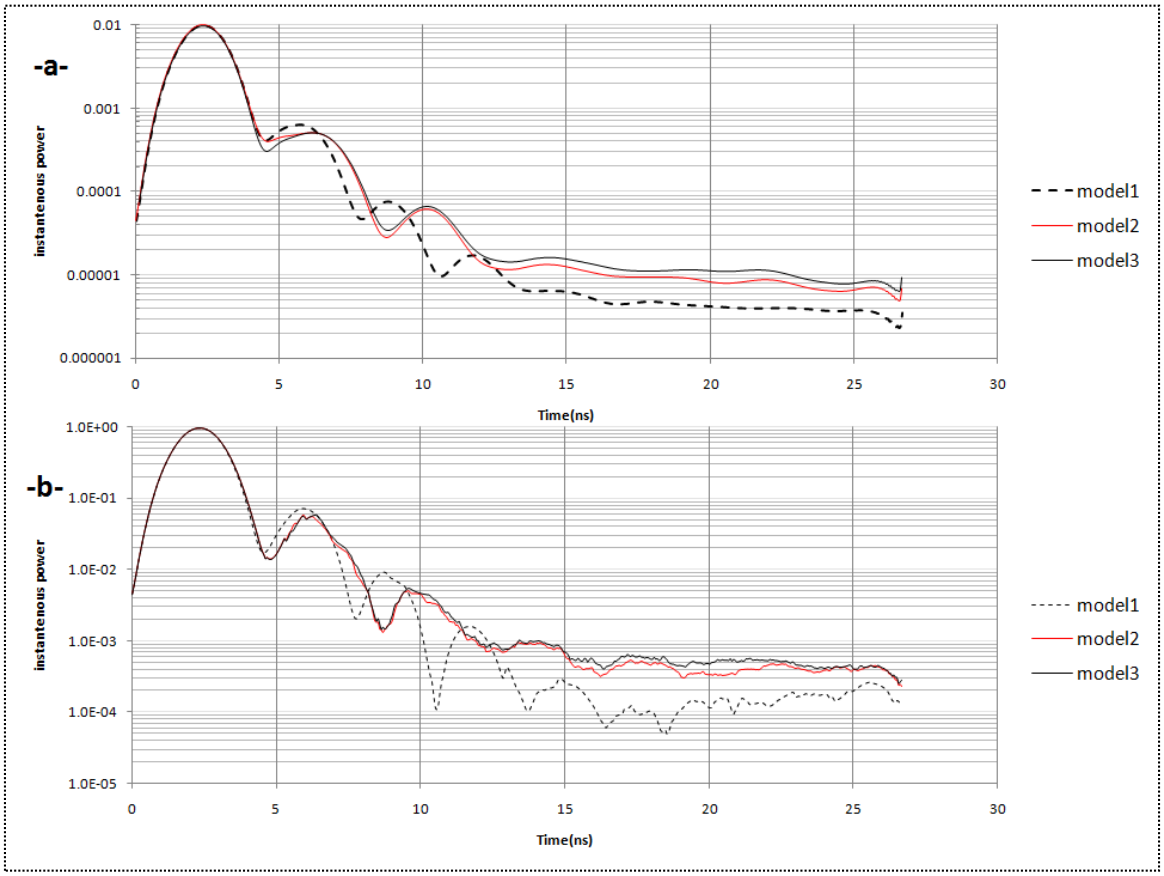

Figure 9: Attenuation of electromagnetic wave as function of time,-a- mean attenuation,-b- median attenuation.

Conclusion and Recommendation:

The essence of this work is neither to supersede GPR real data nor to supplement the actual interpretation of specific data. It is rather integral part and can be instigated as needed. To sum up, we would like to point out:

1- The modeling was successful and the assigned values of dielectric constant and conductivity to the models showed significant level of correlation that can be matched with real data acquired in area nearby.
2- The modeling unfolds the difference in the nature of the reflection with and without surface roughness.
3- Being the sole factor altered in the simulation, roughness can cause severe perturbations and reduce penetration depth of electromagnetic wave.
4- It might be advantageous to attempt simulation of several GPR profiles across the site in figure 1-III-. Keeping the same assumption with roughness added, these profiles can be later viewed as 3D dataset using time slice or isosurface rendering.

Acknowledgement:

We would like to thank all people from Department of Geology, University of Basrah, who participated in acquisition of ground penetrating radar profiles, especially Dr. Badir N. Al Badran for allocating the testing data for the scientific research, Dr. Emad Al Khersan for handling early acquisition parameters and Dr. Ali AL Mayahi for his consent to use the test data for publishing.

REFERENCES

1. Al Bahadily, Hayder; Yousif, Manaf A;. (2012). Magnetic Survey for Detection of Buried Archaeological Features in Al Madai'n Area, Southeast of Baghdad, Iraq. *Iraqi Bulletin of Geology and Mining , 8* (1), 47-58.

2. Atea, A M; Bana, D S; Mutasher, W R; Flayh, Q M;. (2007). Simulation of Influence of Artificial Recharge on Ground Water Elevations of Sandy Dibdiba Formation in Safwan Region, Southern Iraq. *Basrah Journal of Science , 27* (1), 17-27(in arabic).

3.Daniels, D. J. (2004). *Ground Penetrating Radar* (second ed.). London, UK: The Institution of Electrical Engineers.

4.Faruk, N., & Gana, U. M. (2103). FDTD Modelling of Electromagnetic Waves in Stratified Medium. *Global Journal of Engineering Research , 12*, 1-12.

5.Goodman, D., & Piro, S. (2013). Geotechnologies and the Environment. *GPR Remote Sensing in Archaeology , 9* . Springer.

6.Jol, H. M. (2009). *Ground Penetrating Radar:Theory and Application* (first ed.). ELSEVIER.

7.Mahmoud, Hussein Marey; Kaniranis, Nikolaos; Stratis, John;. (2010). Salt Damage on The Wall Paintings of The Festival Templeof THUTMOSIS III, Karnak Temples Complex, Upper Egypt. A case study. *International Journal of Conservative Science , 1* (3), 133-142.

8.NCCI. (2010). *Basrah Governrate Profile.* Report, Basrah.

9.Sabti, Ali Z; Mutasher, Wissam R;. (2006). Detection of Archaeological Structures at Ancient Basrah City by Assistant of Electrical Resistivity Method. *Basrah Research Journal(science) , 32* (3), 7-15 (in arabic).

10.Sadiku, M. N. (2001). *Numerical Techniques in Electromagnetics* (second ed.). USA: CRC Press.

11.Sharma, P. V. (2004). *Environmental and Engineering Geophysics.* Edinburgh: Cambridge University Press.

12.Taflove, A., & Hagness, S. C. (2000). *Computational Electrodynamics:The Finite Difference Time-Domain Method* (second ed.). Norwood, USA: The ARTECH HOUSE.

13.Ullrich, Burkart; Gunther, Thomas; Rucker, Carsten;. (2007). Electric Resistivity Tomography Methods for Archaeological Prospection. *Computer Applications and Quantitative Methods in Archaeology* (02).